JOURNAL OF VIROLOGY, Aug. 2008, p. 7988–7999 Vol. 82, No. 16
0022-538X/08/$08.00+0 doi:10.1128/JVI.00894-08

A Novel Cellular Protein, VPEF, Facilitates Vaccinia Virus Penetration into HeLa Cells through Fluid Phase Endocytosis▽†

Cheng-Yen Huang, Tsai-Yi Lu, Chi-Horng Bair,‡ Yuan-Shau Chang,§ Jeng-Kuan Jwo, and Wen Chang*

Institute of Molecular Biology, Academia Sinica, 128, Sec. 2, Academia Rd., Nankang, Taipei 11529, Taiwan, Republic of China

Received 28 April 2008/Accepted 2 June 2008

Vaccinia virus is a large DNA virus that infects many cell cultures in vitro and animal species in vivo. Although it has been used widely as a vaccine, its cell entry pathway remains unclear. In this study, we showed that vaccinia virus intracellular mature virions bound to the filopodia of HeLa cells and moved toward the cell body and entered the cell through an endocytic route that required a dynamin-mediated pathway but not a clathrin- or caveola-mediated pathway. Moreover, virus penetration required a novel cellular protein, vaccinia virus penetration factor (VPEF). VPEF was detected on cell surface lipid rafts and on vesicle-like structures in the cytoplasm. Both vaccinia virus and dextran transiently colocalized with VPEF, and, importantly, knockdown of VPEF expression blocked vaccinia virus penetration as well as intracellular transport of dextran, suggesting that VPEF mediates vaccinia virus entry through a fluid uptake endocytosis process in HeLa cells. Intracellular VPEF-containing vesicles did not colocalize with Rab5a or caveolin but partially colocalized with Rab11, supporting the idea that VPEF plays a role in vesicle trafficking and recycling in HeLa cells. In summary, this study characterized the mechanism by which vaccinia virus enters HeLa cells and identified a cellular factor, VPEF, that is exploited by vaccinia virus for cell entry through fluid phase endocytosis.

The poxviruses form a group of large DNA viruses that includes variola virus, the causative agent of smallpox disease. Though smallpox itself has been eradicated, the fear of biological warfare and the recent occurrence of accidental monkeypox virus transmission between species (22) and of eczema vaccinatum (33) have alerted us to the potential danger of new emerging diseases. In addition, the potential applications of poxviruses as improved vaccines (34) and as oncolytic agents for cancer therapy (57) have raised new interest in poxvirus biology.

Vaccinia virus, the well-studied prototype of the *Orthopoxvirus* genus in the family *Poxviridae*, has a wide range of infectivity in many cell lines and animals (20). It produces several forms of infectious particles, of which the vaccinia intracellular mature virus (IMV) is the most abundant in cells (see reference 14 and references therein). An IMV is enclosed by a single envelope and contains more than 70 viral proteins (11, 45, 65).

The molecular mechanism of vaccinia IMV entry remains largely unknown. IMV binds to ubiquitous cellular attachment factors, such as glycosaminoglycans (12, 27) and the extracellular matrix protein laminin (10). It is not known whether IMV recognizes additional cellular coreceptors to trigger the post-binding fusion step, although virus entry through fusion with the plasma membrane (3, 9, 19, 37) or intracellular compartments (16, 58) has been reported. Interestingly, IMV has been shown to trigger cellular signaling during virus entry (2, 37, 44), but the molecular pathway of virus uptake has not been characterized.

In this study, we characterized the mechanism by which vaccinia virus enters HeLa cells and investigated cellular factors that are important for vaccinia virus entry.

MATERIALS AND METHODS

Reagents, cells, plasmid vectors, and viruses. HeLa cells were cultured in Dulbecco's modified Eagle medium (DMEM) supplemented with 10% fetal bovine serum. The wild-type WR strain of vaccinia virus was used. IMV virions were purified on a 36% sucrose cushion, followed by 25 to 40% sucrose gradient centrifugation as described previously (32), and stored at −70°C. Purified rabbit anti-VPEF immunoglobulin G (IgG), purchased from QCB (Hopkinton, MA), was raised against a peptide sequence of VPEF (KSTGVFQDEELLFSHKLQ KDNDPD) which is conserved in human, mouse, and CHO cells. Rabbit anti-A4L antiserum was raised against recombinant A4L protein purified from bacteria. Rabbit anti-vaccinia virus antiserum was raised against IMVs. The mouse monoclonal antibody (MAb) clone 2D5, recognizing the L1R protein, was obtained from Y. Ichihashi (30). A mouse anti-human transferrin receptor (TfR) MAb was purchased from Zymed Laboratories, Inc. Rabbit anti-TfR antibodies (Abs) were purchased from Chemicon and Millipore. Mouse anti-CD107a (Lamp1) Abs and rabbit anticaveolin Abs were purchased from BD Biosciences Inc. Mouse anticaveolin MAb was purchased from BD Transduction Laboratories Inc. Tetramethylrhodamine-conjugated goat anti-rabbit IgG Abs were purchased from Invitrogen. Cy5-conjugated goat anti-mouse IgG Abs were purchased from Jackson ImmunoResearch Laboratories, Inc. The cholera toxin B subunit (CTB) conjugated to Alexa Fluor 594, Texas Red- or fluorescein isothiocyanate (FITC)-conjugated transferrin, and Texas Red- or FITC-conjugated dextran (molecular weight, 10,000) were purchased from Molecular Probes and Invitrogen. The pEGFP-C1 vector was purchased from Clontech Inc. The Rab11 plasmid was purchased from Missouri S&T cDNA Resource Center (Rolla, MO). Eps15D95/295 was provided by Alice Dautry-Varsat (L'Institut Pasteur, Paris, France). Plasmids encoding wild-type dynamin 1 (WT-Dyn1), dynamin 1 with a K44A mutation (DN-dyn1 [Dyn1K44A]), WT-Dyn2, and DN-dyn2 (Dyn2K44A) were from Sandra Schmid (Scripps Research Institute, CA). pEGFP-C3-Rab5 was provided by Marino Zerial (Max Planck Institute, Ger-

* Corresponding author. Mailing address: Institute of Molecular Biology, Academia Sinica, 128, Sec. 2, Academia Rd., Nankang, Taipei 11529, Taiwan, Republic of China. Phone: 886-2-2789-9230. Fax: 886-2-2782-6085. E-mail: mbwen@ccvax.sinica.edu.tw.

† Supplemental material for this article may be found at http://jvi.asm.org/.

‡ Present address: Hsinchu Science Park, Jhunan, Miaoli County, Taiwan, Republic of China.

§ Deceased.

▽ Published ahead of print on 11 June 2008.

many). The mCherry plasmid was obtained from Roger Y. Tsien (Howard Hughes Medical Institute, University of California at San Diego). Dynasore was a gift from Tomas Kirchhausen (Harvard Medical School and the CBR Institute for Biomedical Research, Inc., MA).

Construction of a fluorescent recombinant vaccinia virus expressing the core protein A4L fused to mCherry (mCherry-VV). (i) Plasmid construction. Fusion of mCherry to the N terminus of A4L was achieved by PCR splicing by overlap extension (25) using vaccinia virus strain WR genomic DNA as the template. Oligonucleotides 1, 5′-CTCCGTTGAATTCGATGACTATAGGACAAGAACCCTCCTC-3′, and 2, 5′-ATCCTCCTCGCCCTTGCTCACCATTTAAGGCTTTAAAATTGAATTGCG-3′, were used to generate a 463-bp PCR product located upstream of the A4L gene open reading frame (ORF). Oligonucleotides 3, 5′-GGCATGGACGAGCTGTACAAGGACTTCTTTAACAAGTTCTCACAGGGG-3′, and 4, 5′-CGTACTCCAAGCTTGTGTAGATGCTACTTCGTCGATGG-3′, were used to generate a 1,215-bp PCR fragment containing the A4L gene ORF and the 346 bp downstream of the A4L gene ORF. The mCherry gene ORF was amplified using pmCherry (51) as the template and oligonucleotides 5, 5′-ATGGTGAGCAAGGGCGAGGAGGAT-3′, and 6, 5′-CTTGTACAGCTCGTCCATGCC-3′, generating a 711-bp fragment. Oligonucleotides 1 and 4 introduced EcoRI and HindIII restriction sites, respectively (underlined), while oligonucleotides 2 and 3 contained mCherry gene sequences enabling the individual fragments to be assembled into a single 2,389-bp gene. This PCR product was cloned into TOPO pCDNA3.1 to form pA4L-mCherry-N.

(ii) Recombinant virus selection. 293T cells were infected with vaccinia virus WR at 5 PFU per cell and transfected using Lipofectamine (Invitrogen) with the DNA fragment produced by EcoRI and HindIII digestion of pA5L-EGFP-N. The cell lysates were collected at 24 h postinfection. Recombinant viruses expressing mCherry were identified by fluorescence and subsequently underwent three rounds of plaque purification on BSC-40 cells.

Time-lapse microscopy. HeLa cells grown to 70% confluence on coverslips were infected at 100 PFU/cell at 37°C for 30 min with purified A4L-mCherry-expressing IMV. Where indicated (see the Fig. 1 legend), 0.5 μM latrunculin A (Invitrogen) and 2.5 μM taxol (Sigma) were added for 30 min at 37°C before and during virus infection. The cells were maintained in dishes in DMEM without phenol red medium (Gibco-Invitrogen); the dishes were placed on a microscope stage for preheating to 37°C in 5% CO_2 before virus addition. The cells were observed on a Zeiss Axiovert 200 M microscope with a ×63, 1.25-numerical-aperture Plan-NEOFluar oil lens using Zeiss AxioVision Rel. 4.6 software. Images were acquired at 30-s intervals for 60 frames at times between 0 and 30 min postinfection.

Isolation of VPEF cDNA by MAb B2 screening of a cDNA phagemid expression library. Cellular mRNA was isolated from total RNA purified from CHO cells using oligo(dT) beads as described previously (47a) and was used to generate a cDNA phagemid expression library in a lambda ZAP vector as described by the manufacturer (Stratagene cDNA synthesis kit) (52). Screening with MAb B2 (4) for a cDNA gene product was performed as described previously (52). Out of 2 million clones, identical cDNA clones were repeatedly isolated, and their sequences were determined. The cDNA was 4.2 kb and contained a full-length VPEF gene ORF that was fused in frame with the coding sequence for the upstream N-terminal portion of lacZ in the ZAP vector, confirming the validity of Ab screening. The VPEF gene ORF encoded a polypeptide of 1,318 amino acids. Its homologues were found in other species, such as humans (KIAA0592) and mice (NM_026585).

To generate a glutathione *S*-transferase (GST)–VPEF fusion construct, the VPEF cDNA was digested with SalI to release the insert VPEF cDNA, which was subcloned into pGEN-KG to generate the GST-VPEF plasmid (12). To generate the VPEF-green fluorescent protein (GFP) construct, the full-length cDNA was PCR amplified and cloned in frame into TOPO vector pcDNA3.1/CT-GFP (Invitrogen) so that GFP was fused at the C terminus. Sequencing was performed to ensure that no mutation was introduced during PCR. Wild-type caveolin-1 DNA was generated by reverse transcription-PCR and cloned into pcDNA3.1/CT-GFP to give the caveolin-GFP plasmid. Construct Cav1Δ1-81 DNA was generated as described previously for construct DN-Cav3 (47).

Soluble protein expression and purification. For protein expression, *Escherichia coli* strain BL21(DE3) was transformed with GST-VPEF or control GST plasmids and then the cultures were induced with 0.2 mM isopropyl-β-D-thiogalactopyranoside (IPTG) for 20 h at 17°C and harvested. GST and GST-VPEF fusion proteins were purified using glutathione beads as described previously (12). The purified proteins were dialyzed against phosphate-buffered saline (PBS) at 4°C and concentrated on Amicon ultracentrifugal filters (Millipore) before use.

Electron microscopy of IMV entry into HeLa cells. Cell morphology during vaccinia IMV entry into HeLa cells was monitored as described previously, with some modifications (31). A suspension of purified wild type IMVs (200 PFU/cell) or G3 mutant IMVs in 0.3 ml of DMEM was applied to a HeLa monolayer in a 12-well tissue culture plate that had been equilibrated for 30 min at 4°C. The plate was placed in a (no. 5782) bucket in a GP8R centrifuge (International Equipment Company), and virus was pelleted onto the cells at 350 × *g* for 1 h at 4°C. Subsequently, the cells were cultured in normal medium at 37°C for 0, 5, 15, or 30 min before fixation. The fixed cells were treated with 1% OsO_4, dehydrated, and embedded as described previously (56). After embedding, the cells were stained with uranyl acetate and lead citrate and analyzed under a Zeiss 902 transmission electron microscope (46).

Confocal immunofluorescence microscopy. (i) Virion binding and penetration assays. The virion binding assay measuring the amount of cell surface-bound virions was performed as described previously (13, 50, 63). The virion penetration assay measuring the intracellular uncoated cores, which can be stained only with anti-A4 core Abs after virus entry, was also performed as described previously (13, 49, 62). In brief, HeLa cells were infected for 1 h at 4°C with wild-type virus at a multiplicity of infection (MOI) of 40 PFU/cell, washed three times with PBS, and either fixed immediately (for the virion binding assay) or incubated for 2 h at 37°C in the presence of cycloheximide (30 μg/ml) and then fixed (for the virus penetration assay). The cells were fixed, permeabilized in PBS–0.2% saponin, and stained with rabbit anti-A4L Abs or mouse anti-L1R MAb, followed by FITC-conjugated goat anti-rabbit IgG Abs or Cy5-conjugated goat anti-mouse IgG Abs, respectively. DNA was visualized by staining with 0.5 μg/ml of DAPI (4′,6-diamidino-2-phenylindole dihydrochloride; Molecular Probes). Cell images were collected with an LSM510 Meta confocal laser scanning microscope (Carl Zeiss, Germany) using a 63× objective lens and confocal microscopy software (release 2.8; Carl Zeiss). The fluorescent particles were counted from multiple photos, and the averaged numbers of surface-bound virions and uncoated cores per cell were determined.

(ii) Soluble protein blocking assay. Fifty, 100, or 200 μg/ml of GST or GST-VPEF was preincubated with virus (MOI = 40) at 4°C for 30 min. The mixture was then added to HeLa cells to initiate virus infection at 4°C for 60 min (for virus binding assays) or at 37°C for 2 h (for the penetration assay). These cells were washed, fixed and stained for viral L1 and core protein as described above for virion binding and penetration assays (11, 49, 61).

(iii) Ab blocking assay. One, 5, 10, or 50 μg/ml of anti-M2 Abs or anti-TfR Abs was preincubated with HeLa cells at 37°C for 1 h, and then the cells were washed with PBS, and used for virus binding and penetration assays as described above for virion binding and penetration assays.

(iv) Patching analyses. Patching of cell surface proteins with Abs was performed as described previously (55). HeLa cells were seeded on coverslips in 12-well plates and then were infected on the next day with vaccinia virus at an MOI of 50 PFU/cell in DMEM for 1 h, washed, and transferred to 12°C for patching of lipid rafts. The cells were incubated at 12°C for 1 h with a primary Ab (anti-vaccinia virus [diluted 1:500], anti-L1R MAb [diluted 1:400], anti-VPEF [3.3 μg/ml], or anti-TfR [50 μg/ml]) or Alexa Fluor 594-CTB (10 μg/ml) (Molecular Probes, Invitrogen), and then tetramethylrhodamine-conjugated goat anti-rabbit IgG (diluted 1:500) or Cy5-conjugated goat anti-mouse IgG (diluted 1:500) (1.5 mg/ml; Jackson ImmunoResearch Laboratories) was added for 30 min. The cells were then fixed for 5 min with 3.7% paraformaldehyde in PBS on ice and then methanol for 10 min at −20°C, mounted in Vectashield medium (Vector Laboratories, Burlingame, CA), and visualized by confocal laser scanning microscopy with an LSM 5 Pascal instrument (Carl Zeiss) using a 63× objective lenses and accompanying software.

(v) Ligand endocytosis assay. HeLa cells were seeded on coverslips 1 day before the experiment to allow growth to 80% confluence. For transferrin uptake analyses (modified from that in reference 6), cells were starved in serum-free DMEM for 2 h at 37°C and then incubated in complete medium containing 25 μg/ml of Cy5- or Texas Red-conjugated transferrin (Molecular Probes, Invitrogen) at 37°C for 30 min before fixation for confocal microscopy analyses. For CTB and dextran uptake (procedure modified from those in references 5 and 53, respectively), cells were incubated at 37°C in complete medium with 8 μg/ml of Alexa Fluor 594-conjugated CTB or 10 mg/ml of FITC-conjugated dextran (molecular weight, 10,000; Molecular Probes, Invitrogen) for 40 min before fixation for confocal microscopy analyses. Alternatively, these ligand-treated cells were cooled on ice, washed twice with cold PBS, fixed in 4% paraformaldehyde, and permeabilized in PBS–0.2% saponin. Cells were stained with anti-M2 Abs (3.3 μg/ml) at room temperature for 1 h, with tetramethylrhodamine-conjugated goat anti-rabbit IgG Abs (diluted 1:1,000) at room temperature for 30 min, and with 0.5 mg/ml of DAPI.

(vi) Dynasore blocking experiments. HeLa cells were preincubated with 0.8% dimethyl sulfoxide (DMSO) or dynasore (40 μM or 80 μM) in serum-free DMEM at 37°C for 30 min and then directly cooled to 4°C and infected with

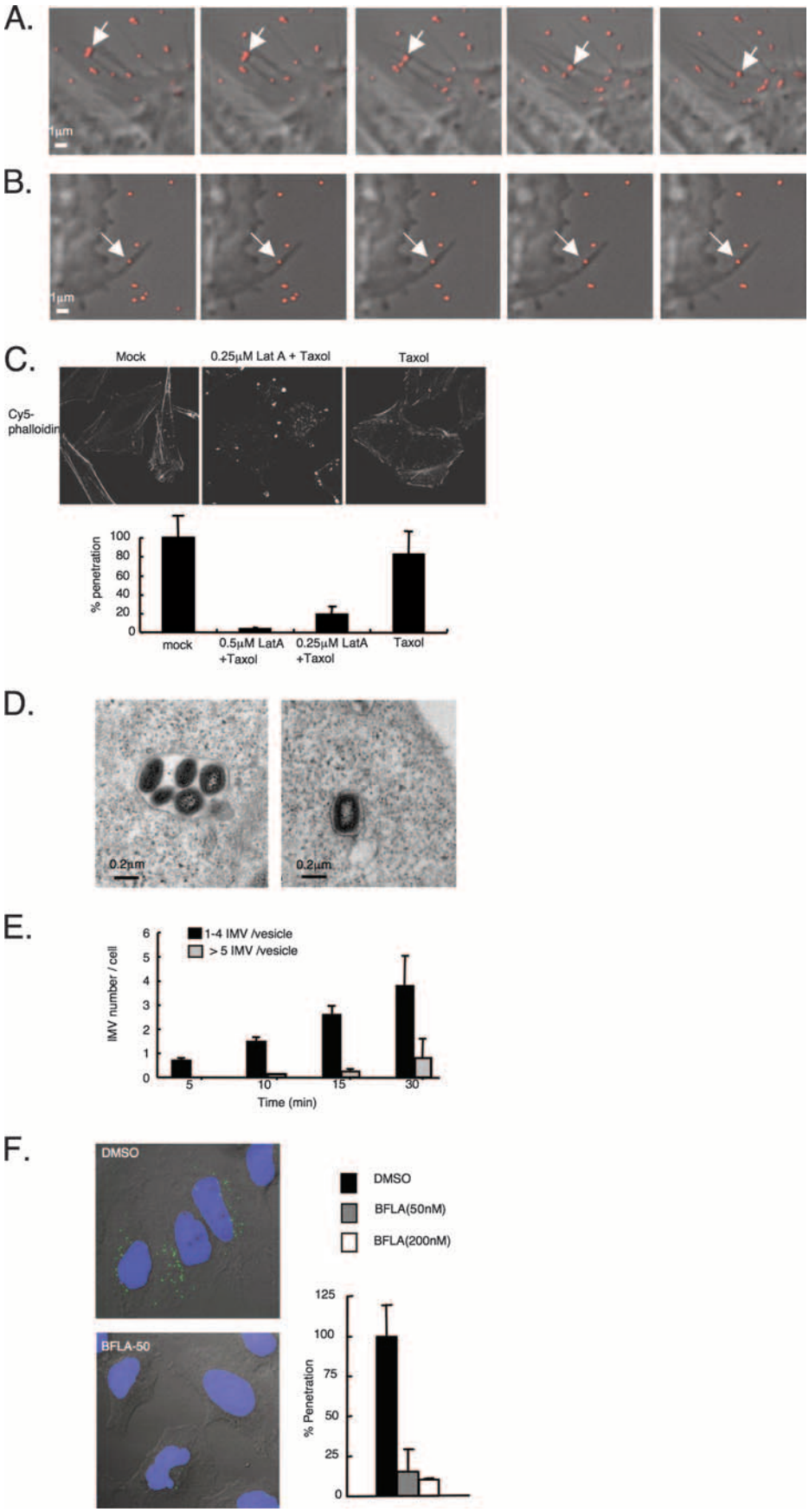
A.
1μm
B.
1μm
C.
Mock
0.25μM Lat A + Taxol
Taxol
Cy5-phalloidin
% penetration
100
80
60
40
20
0
mock
0.5μM LatA +Taxol
0.25μM LatA +Taxol
Taxol
D.
0.2μm
0.2μm
E.
1-4 IMV /vesicle
> 5 IMV /vesicle
IMV number / cell
6
5
4
3
2
1
0
5
10
15
30
Time (min)
F.
DMSO
BFLA-50
DMSO
BFLA(50nM)
BFLA(200nM)
% Penetration
125
100
75
50
25
0

vaccinia IMV (MOI of 40) at 4°C for 1 h. Cells were washed with cold PBS to remove free virions and further incubated at 37°C for 2 h before fixation for virus penetration assays as described above. The drug was present in the medium throughout the experiments. Alternatively, HeLa cells were treated with dynasore as described above and then pulsed with transferrin for a further 30 min before fixation for confocal microscopy and quantification using MetaMorph Offline, version 6.1 (Molecular Devices, CA).

Knockdown of endogenous VPEF expression using siRNA. The control cyclophilin B (CypB) small interfering RNA (siRNA) duplex and the two VPEF siRNA duplexes, 3-378 (AAGUAGAUCUCAUUCCUAAUU) and 1-525 (CA AAGGAUCUAUACAUUGAUU), which, respectively, target the 378 to 398 and 525 to 545 regions of human KIAA0592 RNA, were purchased from Dharmacon Inc. HeLa cells were transfected with siRNA duplexes (50 pM) using Lipofectamine 2000 (Invitrogen), the process was repeated, and then the cells were used for virus binding and penetration assays as described above.

Nucleotide sequence accession number. The VPEF gene ORF was submitted to the NCBI under accession number AAK 53434.

RESULTS

HeLa cells exhibit abundant actin protrusions that provide an efficient means for vaccinia IMV to reach cell bodies before virus entry. We examined the entry pathway of vaccinia IMV into HeLa cells. Electron microscopy (EM) showed that IMVs bound to long and short filopodia (see Fig. S1A in the supplemental material), as previously reported by Locker et al. (37). To understand the relevance of these filopodia to virus entry, we turned to live-cell imaging, which allows a more dynamic observation of the interaction between virus particles and cells. Our attempt to construct a fluorescent vaccinia IMV expressing an envelope protein fused to the mCherry protein (51) was unsuccessful due to loss of infectivity. However, a fluorescent virus expressing the core protein A4L fused to mCherry, named mCherry-VV, was viable and subsequently purified (see Fig. S1B in the supplemental material). Within minutes after infection, some of the inoculated mCherry-VV bound to long filopodia of HeLa cells and started moving along the surface of the filopodia toward the cell body before disappearing at the base of filopodia or out of the focal plane (Fig. 1A; see Movies S1 and S2 in the supplemental material). Some of the viruses bound to cell edges or active ruffling areas and were transported to the cell body during ruffling retraction (see Movie S3 in the supplemental material), whereas other viruses were "grabbed" by waving actin protrusions and brought back to the cell body (see Movie S4 in the supplemental material). When HeLa cells were treated with latrunculin A to interrupt actin polymerization, as described previously (39), IMV attachment to filopodia was not affected; however, many of the bound particles became still (Fig. 1B; see Movie S5 in the supplemental material) or showed only slight local movement, demonstrating the importance of actin dynamics in the regulation of vaccinia IMV movement prior to cell entry. As expected, virus penetration into HeLa cells, as determined by measuring the amount of uncoated core A4L protein using previously described virus penetration assays (62), was significantly inhibited by latrunculin A (Fig. 1C). Taxol, previously reported not to affect vaccinia IMV entry (37), was included here to stabilize microtubules so that cells remained attached to plates, and this drug alone did not affect IMV movement (see Movie S6 in the supplemental material). Together, the results suggest that these dynamic actin-containing structures could serve as effective ways to recruit viruses for cell entry.

Due to the limitations of live-cell imaging, we were unable to follow individual viral particles after they reached the cell body. EM analyses showed that viruses which had reached the cell body were more associated with filopodium-rich surfaces than with smooth surfaces and were surrounded by filopodia (see Fig. S2A in the supplemental material). Interestingly, unlike Locker et al. (37), who reported no evidence of IMVs in endocytic vesicles, we observed single or multiple IMV particles that were enveloped by the intracellular vesicular membrane during viral infection (Fig. 1D), and the number of these vesicles increased steadily over the first 30 min of virus infection (Fig. 1E), suggesting endocytosis of IMVs by HeLa cells. Indeed, we found that viral core exposure was significantly inhibited in HeLa cells treated with bafilomycin (BFLA) (Fig. 1F), which blocks the endocytic route previously reported for virus entry into BSC-1 cells (58). We also used a mutant vaccinia virus in which expression of a component of the viral fusion complex, G3, was under IPTG regulation; mutant G3$^-$ vaccinia viruses prepared from cells without IPTG induction produce IMVs that bind to cells, but the fusion step is blocked (31). In EM analyses, G3$^-$ mutant virions accumulated within the cytoplasmic vesicles, suggesting that endocytic vesicles containing IMVs were already present in cells prior to the membrane fusion step (see Fig. S2B in the supplemental material). Taken together, our results show that vaccinia IMV was able to enter HeLa cells through an endocytic pathway, although we did not exclude plasma membrane fusion, as previously reported (37).

Vaccinia IMV infection of HeLa cells is not mediated by clathrin-coated pits or caveolae. To define which endocytic machinery was used for vaccinia IMV entry, we obtained several dominant-negative (DN) mutant gene constructs known to specifically block different cellular endocytic pathways and tested their ability to block vaccinia IMV entry into HeLa cells.

FIG. 1. Vaccinia IMV entry into HeLa cells. (A) Live-imaging recording of mCherry-VV movement by time-lapse immunofluorescence microscopy. HeLa cells were infected with purified mCherry-VV IMV, and time series images were immediately collected every 30 s. The arrows and red dots show the moving mCherry-VV particles. (B) IMV movement is actin dependent. HeLa cells were pretreated with 0.5 μM latrunculin A and 2.5 μM taxol, infected with mCherry-VV, and recorded as described for panel A. (C) IMV entry requires actin polymerization. (Top) HeLa cells were treated with 2.5 μM taxol alone or 2.5 μM taxol plus 0.25 μM latrunculin A (LatA) as described for panel B, fixed, and stained with Cy5-phalloidin. Taxol was added in these cells to stabilize cell shapes and had no effect on actin polymerization. (Bottom) HeLa cells, treated with LatA as described above were infected with IMV (MOI = 40) at 37°C for 1 h and fixed for virus penetration assays to detect the uncoated viral core in cells. (D) Endocytosed IMV in HeLa cells. (E) Quantification of intravesicular virions, with 10 images for each time point. (F) Penetration of vaccinia IMV into HeLa cells is blocked by BFLA. HeLa cells were pretreated with DMSO, treated with 50 or 200 nM BFLA in DMSO, infected with IMV at 37°C for 60 min, fixed, permeabilized, and stained with anticore A4L (green) Abs and DAPI (blue) as described in Materials and Methods. The photos show merged images of uncoated cores (green) and nuclei (blue) in the infected cells treated with DMSO or 50 nM BFLA (BFLA-50).

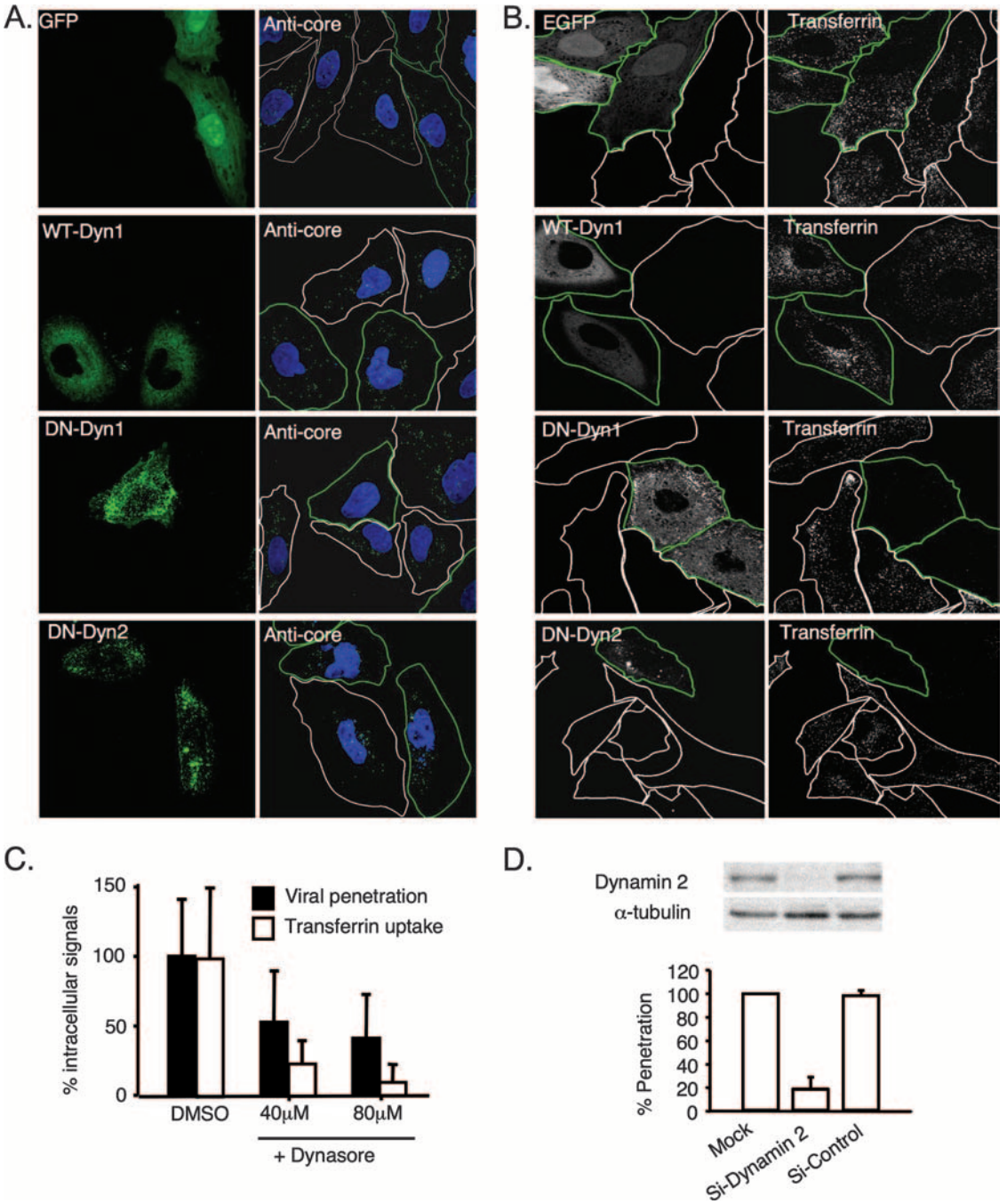

FIG. 2. (A and B) Vaccinia IMV penetration does not require clathrin- or caveola-mediated pathways. HeLa cells were transfected with individual plasmids encoding GFP, GFP-fused WT-Dyn1, DN-Dyn1, or DN-Dyn2, infected with vaccinia virus, fixed, permeabilized, and stained with anticore (anti-A4L) Abs and DAPI. Images were obtained using a Zeiss LSM510 Meta confocal laser scanning microscope. Green and white lines delineate the edges of GFP-expressing or -nonexpressing cells, respectively. (B) Transferrin uptake was blocked by DN-Dyn1 and DN-Dyn2 proteins. HeLa cells were transfected with individual plasmids as described for panel A and assayed for transferrin uptake using confocal immunofluorescence microscopy. Green and white lines were used to delineate the edges of GFP-expressing or -nonexpressing cells, respectively. (C) Dynasore inhibited both vaccinia virus penetration and transferrin uptake. HeLa cells were either mock-treated with DMSO or treated with Dynasore (40 μM or 80 μM) for 30 min and subsequently infected with vaccinia IMV at 37°C. The penetration efficiency of vaccinia virus in dynasore-treated cells was reduced to 52.51% and 41.64%, respectively, of the control level. As expected, transferrin uptake was also reduced in the presence of 40 μM and 80 μM dynasore. (D) Knockdown of endogenous dynamin 2 in HeLa cells blocked vaccinia virus penetration. HeLa cells were either mock-treated (Mock) or treated with nontargeting siRNA (Si-Control) or siRNA targeting dynamin 2 (Si-Dynamin 2) (29) and infected with vaccinia IMV, and virus penetration was determined as previously described (62). The immunoblots showed that dynamin 2 protein level was reduced in the Si-Dynamin 2 knockdown cells. (E) Vaccinia IMV penetration does not require clathrin- or caveola-mediated pathways. HeLa cells were transfected with plasmids expressing GFP-fused DN-Eps15 or DN-Cav1, infected with vaccinia virus, fixed, permeabilized, and stained with anticore (anti-A4L) Abs and DAPI. (F) DN-Eps15 and DN-Cav1 blocked transferrin and CTB uptake, respectively. HeLa cells were transfected with a plasmid expressing DN-Eps15 or DN-Cav1 and assayed for transferrin or CTB uptake using confocal immunofluorescence microscopy. Cells expressing the GFP-fused proteins are marked with green lines, and control cells are marked with white lines. (G) Quantification of the viral penetration of the cells in panels A and E. The A4L cores in each GFP-expressing cell were counted and normalized to the number of A4L cores in nonexpressing cells. In each group, at least 20 GFP-expressing and 20 GFP-nonexpressing cells were counted. The bars represent the standard deviations of three independent experiments. Wt, wild type.

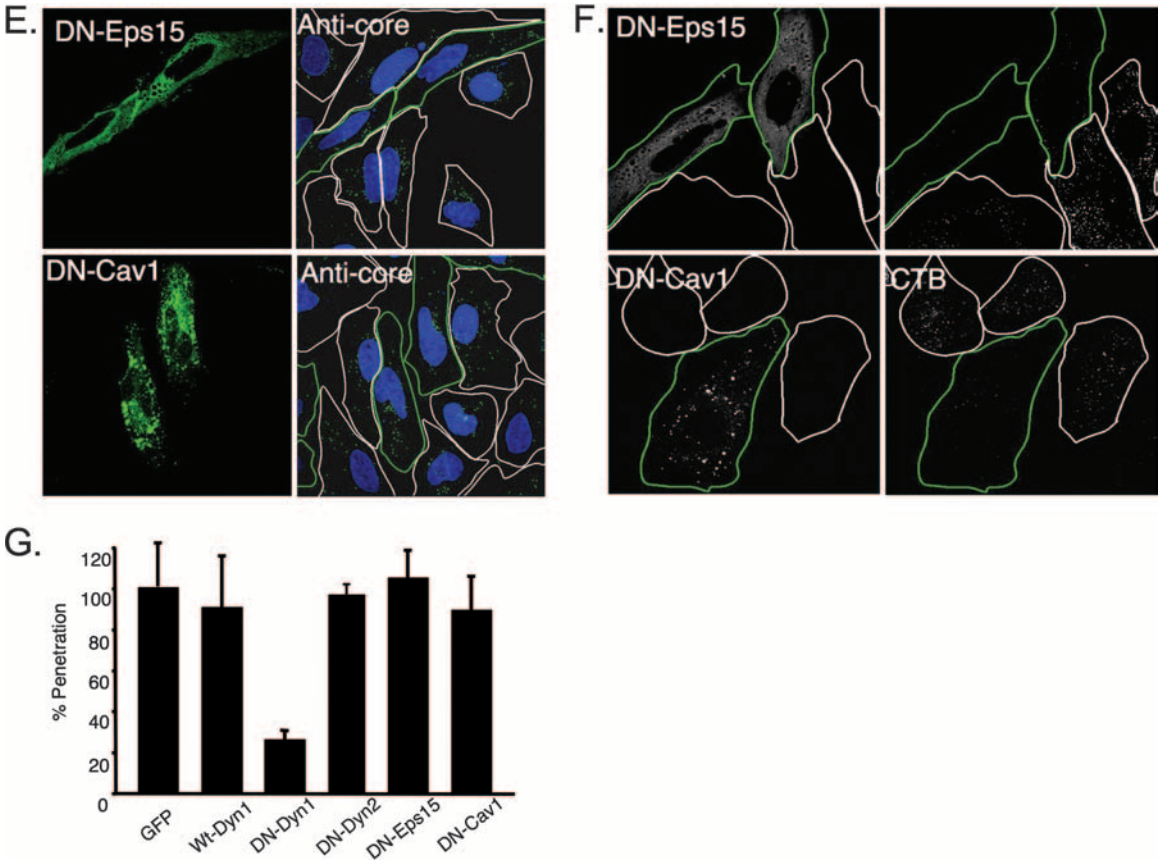

A dynamin 1 K44A DN mutant (DN-Dyn1) unable to bind GTP has been shown to inhibit the function of both endogenous dynamin 1 and dynamin 2 isoforms and to block major endocytic pathways, including clathrin- or caveola-mediated endocytosis, and even fluid phase endocytosis (7, 17, 18, 21, 40, 42, 60). In addition, a K44A mutant dynamin 2 (DN-Dyn2), the isoform that is ubiquitously expressed in nonneuronal cells, was included (15, 54). The more specific DN mutant Eps15 construct (Eps15Δ95/295 [DN-Eps15]), which blocks only clathrin-mediated endocytosis (6), and a DN caveolin construct (Cav1Δ1–81 [DN-Cav1]), which blocks caveola-mediated endocytosis (47), were also included. HeLa cells were transfected with each of these constructs and subsequently infected with vaccinia IMV as described in Materials and Methods; then the cells were fixed, permeabilized, and stained for the presence of intracellular core A4 protein after virus penetration, as described previously (61, 62). Ectopic expression of GFP-fused DN-Dyn1, but not of GFP-fused WT-Dyn1 or DN-Dyn2 or of GFP alone, blocked vaccinia IMV entry by ~70% (Fig. 2A; data are quantified in Fig. 2G). In control experiments, both GFP-fused DN-Dyn1 and DN-Dyn2 effectively blocked uptake of transferrin into HeLa cells (Fig. 2B), showing an isoform-related variation in blockade of IMV entry but not of the coat-mediated endocytosis pathway. To directly inhibit the GTPase activity of endogenous dynamin in HeLa cells, we then treated cells with 40 and 80 μM concentrations of a cell-permeating inhibitor of dynamin, dynasore, that has been shown to specifically interfere with endocytic functions that depend on dynamin without affecting dynamin-independent functions (38). Dynasore blocked transferrin uptake as expected and, more importantly, blocked vaccinia IMV penetration (Fig. 2C). We also knocked down endogenous dynamin 2 expression in HeLa cells using a siRNA approach, and virus penetration was blocked (Fig. 2D). We thus concluded that vaccinia IMV entry into HeLa cells is dynamin dependent. Furthermore, expression of the GFP-fused Eps15Δ95/295 or Cav1Δ1–81 construct had little effect on the amount of uncoated intracellular A4 core protein (Fig. 2E; data are quantified in Fig. 2G), showing that vaccinia IMV does not utilize a clathrin- or caveolin-dependent endocytic pathway. In control experiments, DN-Eps15 and DN-Cav1 readily blocked uptake of transferrin and CTB, respectively, into HeLa cells (Fig. 2F). These results show that vaccinia IMV entry into HeLa cells does not rely on the formation of clathrin-coated pits or caveolae. Instead, IMV has evolved a different strategy for internalization into HeLa cells through an actin- and dynamin-dependent process. Although we could call it "dynamin-dependent macropinocytosis," we feel that "fluid phase endocytosis," as described by Cao et al. (7), fits better to our observation, so we decided to use the latter term. Although fluid phase endocytosis is consistent with active cellular protrusions recruiting viruses observed in our imaging analyses, more data are required to sustain this conclusion.

Colocalization of novel cellular protein VPEF with vaccinia virus during virus penetration into cells through plasma membrane lipid rafts. The molecular demonstration of virus entry

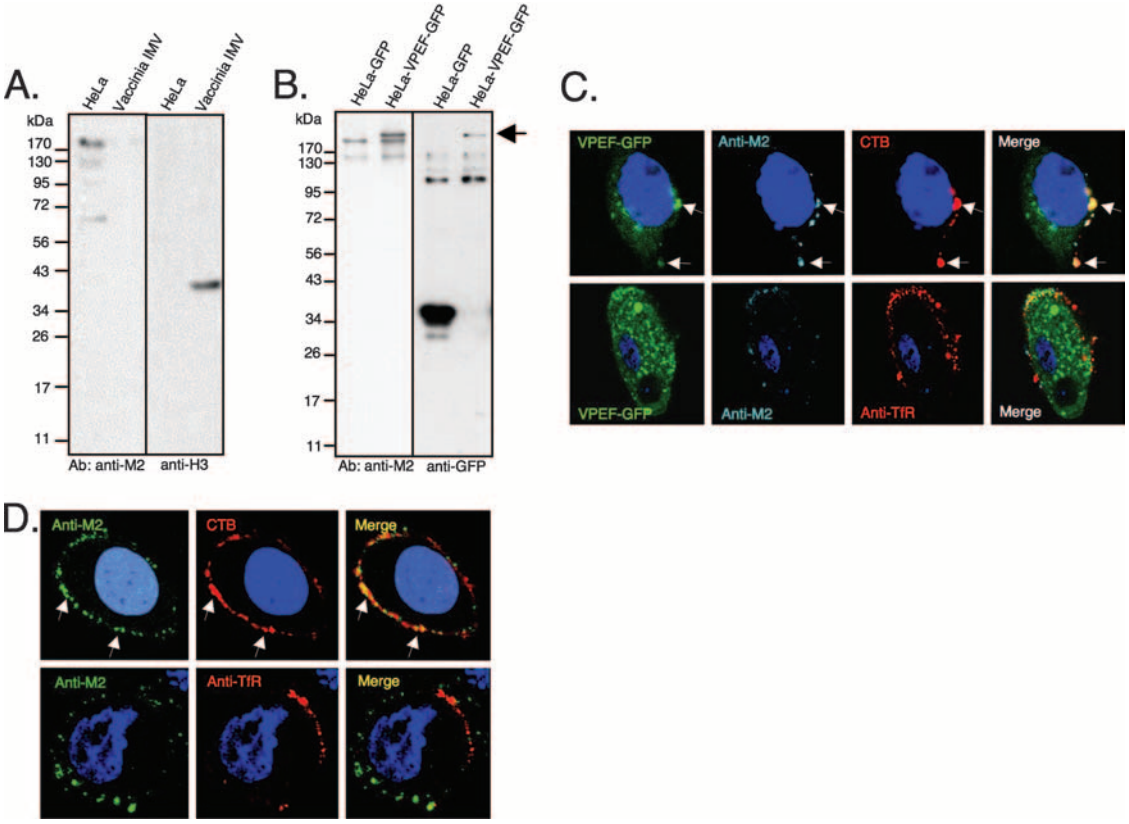

FIG. 3. VPEF protein colocalized with plasma membrane microdomains. (A) Immunoblot analyses of HeLa cell lysates and purified vaccinia virus virions using anti-M2 Abs or anti-H3 (an IMV envelope protein) Abs. (B) Immunoblot analyses of HeLa cells transfected with a plasmid expressing GFP or VPEF-GFP using anti-M2 Abs. Anti-GFP Ab recognized only the exogenous VPEF-GFP (arrow) in HeLa cells. (C) Ectopically expressed VPEF-GFP was present on plasma membrane microdomains. HeLa cells expressing VPEF-GFP were copatched with anti-M2 Abs (cyan) and lipid raft marker CTB (CTB-Alexa Fluor 594, red) or with nonraft marker anti-TfR Abs (red) without permeabilization. The arrows indicate lipid raft regions where VPEF-GFP colocalized with anti-M2 staining and CTB. (D) Endogenous VPEF was present on plasma membrane microdomains. HeLa cells were copatched with anti-M2 Abs (green) and CTB-Alexa Fluor 594 (red) or anti-TfR Abs (red) as described previously (13, 55). The arrows indicate lipid rafts region where VPEF-GFP colocalized with anti-M2 staining and CTB.

pathways often requires the identification of cellular proteins that are important in virus entry. We previously generated MAb B2, which recognizes an unknown cell surface molecule(s) and can block vaccinia IMV infection (4). MAb B2 was used to screen a phage cDNA expression library, where it identified a single CHO cell cDNA clone (accession number AAK 53434) containing a full-length ORF encoding a 1,318-amino-acid protein, which we tentatively named VPEF. VPEF has homologues in other species, including humans (KIAA0592) and mice (NM_026585), but none contain any known structural domains or have a known function. Because MAb B2 is a low-affinity IgM, which gives a high background in immunofluorescence analyses, we generated a rabbit antiserum (anti-M2) using peptide KSTGVFQDEELLFSHKLQK DNDPD (M2) from VPEF. The anti-M2 Abs recognized an endogenous cellular protein with an apparent molecular mass of about 200 kDa on sodium dodecyl sulfate gels and not vaccinia IMV proteins (Fig. 3A). The 200-kDa protein size on gel was consistent with that of the in vitro-translated product of VPEF cDNA (data not shown), although larger than the predicted molecular mass of 145 kDa. The anti-M2 Abs also recognized the ectopically expressed VPEF-GFP fusion protein, but not GFP, transfected in HeLa cells (Fig. 3B). In immunofluorescence analyses, the anti-M2 Abs also reacted specifically with exogenous and endogenous VPEF protein in cytoplasm and not with vaccinia IMV particles (see Fig. S3 in the supplemental material).

Although abundant fluorescence of VPEF-GFP fusion protein appeared as intracellular speckles in HeLa cells, we could enhance the surface detection of VPEF-GFP using the anti-M2 Abs to cross-link surface VPEF-GFP as patches on the plasma membrane (Fig. 3C). Immunofluorescence microscopy showed that these VPEF-GFP-containing patches were colocalized with the plasma membrane lipid raft marker CTB, and not with TfR, suggesting that VPEF-GFP associates with lipid raft microdomains on the plasma membrane (Fig. 3C). Consistent with the data for ectopically expressed VPEF-GFP, endogenous VPEF was also detected on cell surface microdomains (Fig. 3D). It is worth noting that endogenous VPEF was present in, but not limited to, microdomains, as VPEF also exhibited intracellular-vesicle-like staining in permeabilized cells (see Fig. S3 in the supplemental material).

We had previously demonstrated vaccinia virus clustering at plasma membrane lipid rafts during virus penetration (13). Since VPEF-GFP was also present on lipid rafts, we investigated whether VPEF-GFP protein colocalized with vaccinia

IMV particles during cell entry. Immunofluorescence analyses showed that VPEF-GFP colocalized mostly with IMVs that stained positive for core protein, suggesting that these IMVs were in the process of penetration (Fig. 4A). To eliminate the possibility that the observed viral core staining was an artifact of virion rupture during cell fixation, we performed kinetic analyses of vaccinia IMV infection in VPEF-GFP-transfected HeLa cells. Cells were infected with vaccinia IMV for 60 min at 4°C and, after a wash to remove unbound virus, were incubated at 37°C for a range of time periods from 0 to 2 h and then harvested for copatching analyses with anti-vaccinia virus and anticore Abs (Fig. 4B; data are quantified in Fig. 4C) as described previously (13). Cycloheximide was added to the medium to block viral early gene expression so that the virus life cycle was arrested immediately after entry (13, 61). At 0 min, as expected, >95% of bound IMV particles were intact and stained negative for core proteins. Initially, only little colocalization between IMV and VPEF was detected (Fig. 4C, left). As virus penetration progressed at 37°C from 30 min to 2 h, less IMV remained on the cell surface and more and more viral signals indicative of penetration intermediates were detected, i.e., cells stained positive with both anti-L1 and anticore Abs (Fig. 4C, middle). Interestingly, most of these penetration intermediates were also associated with VPEF. After penetration, viral cores were no longer associated with the viral envelope (Fig. 4C, right). The majority of these uncoated cores were not colocalized with VPEF, suggesting a transient association of VPEF with IMV during virus entry and a possible role of VPEF in IMV penetration.

Cellular VPEF is required for vaccinia virus penetration into HeLa cells. To test whether VPEF is important for vaccinia virus entry into cells, recombinant GST-VPEF fusion protein was expressed in *E. coli* and tested for its ability to block vaccinia virus entry into cells. Vaccinia IMV binding to cells was not affected by GST-VPEF or GST, whereas heparin readily blocked virus attachment as expected (Fig. 5A; see Fig. S4A in the supplemental material). In contrast, GST-VPEF, but not control GST, blocked vaccinia virus core uncoating in a concentration-dependent manner (Fig. 5A; see Fig. S4B in the supplemental material), suggesting that VPEF plays a role in the postattachment penetration step. Although the GST-VPEF blocking effect was only partial at the highest dosage used (200 μg/ml), its blocking activity was comparable to those of several other recombinant viral envelope proteins previously used in virus entry blocking assays (26, 28). The anti-M2 Abs were used in further experiments similar to those above (Fig. 5B), which showed that, while control anti-TfR Abs did not block vaccinia IMV entry, anti-M2 Abs effectively reduced IMV penetration without affecting virus binding to cells, consistent with the results of the soluble protein blocking assays.

To determine if endogenous VPEF is required for vaccinia virus infection of permissive HeLa cells, siRNAs targeting human VPEF were transfected into HeLa cells to silence endogenous VPEF expression (VPEF-KD cells). In immunoblot analyses, a pool of four siRNAs (mix) and the single siRNA 3-378 both effectively reduced VPEF levels, whereas another siRNA, 1-525, had only a slight effect (Fig. 5C). Cellular CypB was independently knocked down as a control (Cyp-KD cells). Vaccinia IMV attachment to either VPEF-KD or CypB-KD cells was not affected (Fig. 5D; see Fig. S4C in the supplemental material), whereas vaccinia virus penetration was significantly reduced in VPEF-KD 3-378-treated cells, mildly reduced in VPEF-KD 1-525-treated cells, and not affected in CypB-KD cells (Fig. 5D; see Fig. S4D in the supplemental material). Quantitatively, more-effective siRNA silencing of VPEF expression resulted in less vaccinia virus penetration.

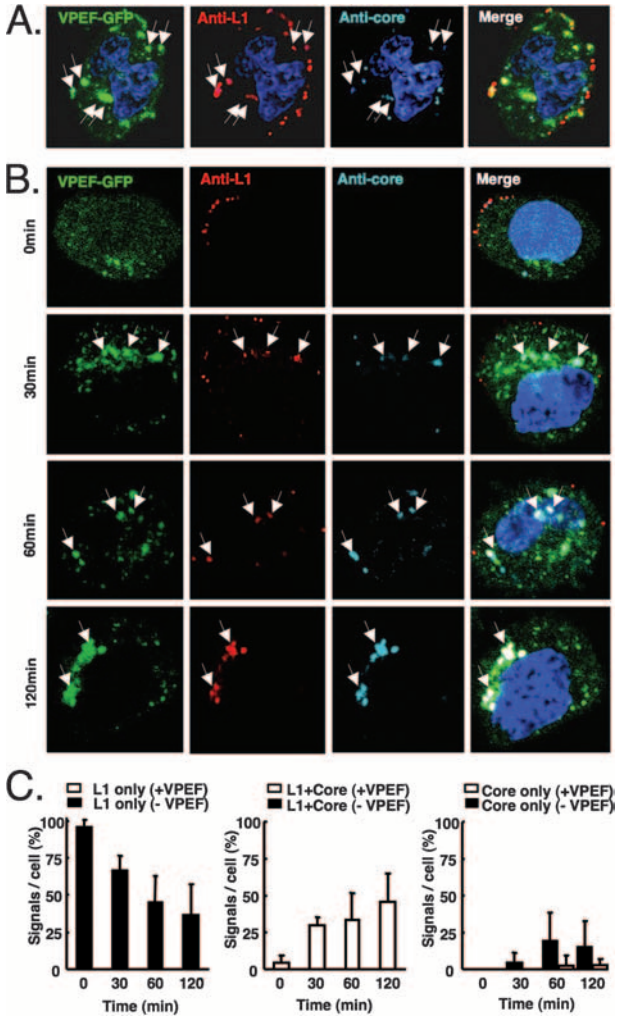

FIG. 4. Transient association of IMV with VPEF during virus penetration. (A) HeLa cells expressing VPEF-GFP were infected with vaccinia IMV at 37°C for 2 h, patched with anti-L1 MAb (red), and then fixed and stained with anticore Ab (Anti-A4L, cyan). The uncoating virions associated with VPEF-GFP, anti-L1, and anticore staining are indicated by arrows. (B) Kinetic analyses of penetrating viruses associated with VPEF-GFP. HeLa cells were infected with IMV, harvested at each time point, and processed for virus penetration assays as described in Materials and Methods. The arrows show colocalization of staining. (C) Quantification of data from panel B. Fluorescent viral signals from all the *z* sections (1-μm thickness) of single cells for a total of 20 cells at each time point were counted. Viral signals were classified in this study as follows. The L1-only signals represent intact bound IMV. The L1 plus core signals represent viral penetration intermediates. The core-only signals represent intracellular viral cores after penetration. The white bars represent viral signals colocalized with VPEF, and the black bars represent viral signals not colocalized with VPEF.

VPEF participates in intracellular transport of dextran in fluid phase endocytosis. Our above results suggested that IMV

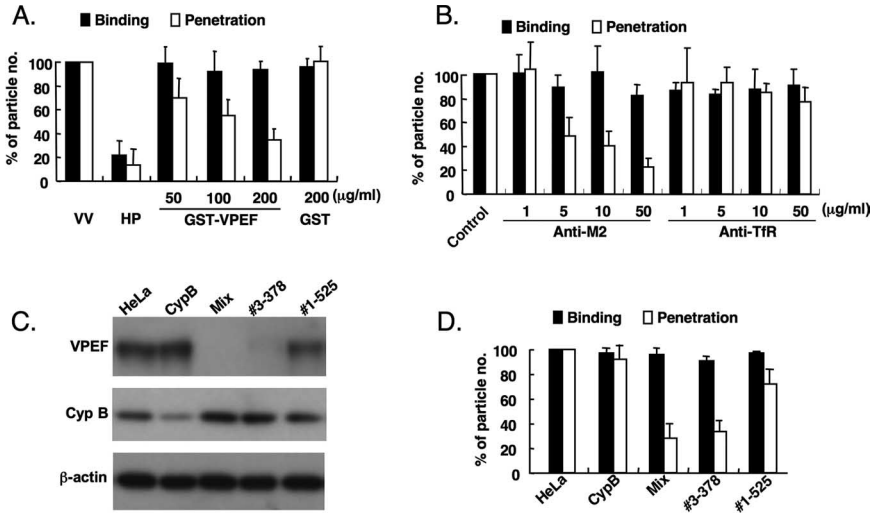

FIG. 5. VPEF protein is important for vaccinia IMV penetration into HeLa cells. (A) Soluble VPEF protein blocked vaccinia IMV penetration into HeLa cells. Purified IMVs (VV) were preincubated at 4°C for 60 min with heparin (HP) (100 μg/ml), control GST (200 μg/ml), or GST-VPEF (50, 100, or 200 μg/ml) and then were used to infect HeLa cells at 4°C for virion binding or at 37°C for virus penetration analysis. Data were obtained from 40 cells at each concentration of the GST proteins used, and experiments were repeated three times. (B) Anti-M2 Abs blocked vaccinia IMV penetration into HeLa cells. HeLa cells were pretreated with anti-M2 Abs or control anti-TfR Abs, washed, and analyzed for virion binding or penetration. (C) Immunoblots of HeLa lysates prepared from knockdown cells transfected with CypB siRNA, a VPEF siRNA mixture (mix), or individual VPEF siRNAs (3-378 or 1-525) and incubated with Abs against VPEF, cyclophilin B, or control β-actin. (D) Quantification of virion binding and penetration assays of knockdown cells.

penetration into HeLa cells may operate through a fluid phase endocytic pathway and that VPEF is important for cellular penetration by IMV. Furthermore, the intracellular distribution of endogenous VPEF was reminiscent of that of intracellular vesicles, suggesting that VPEF may be part of the system for vesicle transport between the cell surface and intracellular organelles. Could it be that the vaccinia IMV somehow recruits and/or diverts a cellular vesicle protein for its own benefit? We hypothesized that the cellular function of VPEF is involved in the uptake or transport of certain physiological ligands. To test this, we incubated HeLa cells with either fluorescence-labeled transferrin or dextran. Transferrin undergoes clathrin-mediated endocytosis, whereas dextran is taken up by fluid phase endocytosis (7, 64). Each of these fluorescent ligands was added to HeLa cells, which were then fixed, permeabilized, and stained with anti-M2 Abs. Transferrin showed little colocalization with VPEF, whereas dextran exhibited clear colocalization with intracellular VPEF (Fig. 6A) 40 min after addition. Four hours later, when the dextran had been chased into late endosomes/lysosomes, no colocalization between dextran and VPEF was observed (Fig. 6B), suggesting that dextran was transported in VPEF-containing vesicles during the early phase after being taken up into HeLa cells. Most importantly, when VPEF expression was knocked down using siRNA, dextran transport in cells was affected, showing a more restricted pattern close to the perinuclear areas (Fig. 6C), suggesting again that VPEF plays a role in the regulation of the fluid phase endocytic pathway in HeLa cells.

To further characterize the membrane organization of the VPEF-containing vesicles, we tested several intracellular vesicle markers: Rab5 for early endosomes (48), caveolin-1 for caveolae/caveosomes (43), and Rab11a for recycling endosomes (59). The VPEF-containing vesicles did not colocalize with Rab5 (Fig. 7A) or caveolin-1 (Fig. 7B) but showed a partial colocalization with the recycling endosome marker Rab11a (Fig. 7C), supporting our hypothesis that VPEF-containing vesicles are distinct from early endosomes and caveolae/caveosomes and participate in vesicle recycling between the cell surface and intracellular organelles. Finally, though both cellular VPEF and dynamin are important for vaccinia virus penetration, immunofluorescence studies revealed no colocalization of VPEF protein with either WT-Dyn1 or DN-Dyn1 and DN-Dyn2 in HeLa cells (Fig. 8), implying that VPEF and dynamin mediate IMV penetration through different mechanisms.

DISCUSSION

We characterized vaccinia IMV entry into HeLa cells and showed that the virus infection process has several interesting features. First, vaccinia IMV required actin polymerization prior to cell entry. That virus "surfing" requires normal actin dynamics has been reported for some retroviruses and vesicular stomatitis virus (36). Surfing may turn out to be a common transport mechanism shared by many viruses if vaccinia virus is added to the list of those using it. Plasma membrane ruffling and actin protrusions regulated by actin dynamics were also involved in vaccinia IMV recruitment. Next, we showed that IMV particles were endocytosed into HeLa cells in a manner independent of clathrin- and caveola-mediated pathways but dependent on dynamin, suggesting a virus entry pathway through fluid phase endocytosis (7). The role of endogenous dynamin 2 in vaccinia IMV entry into HeLa cells was demonstrated using three experimental approaches, first with an expressed DN-Dyn1 isoform, next with a dynamin-specific inhibitor, dynasore, and finally with a siRNA approach. In our

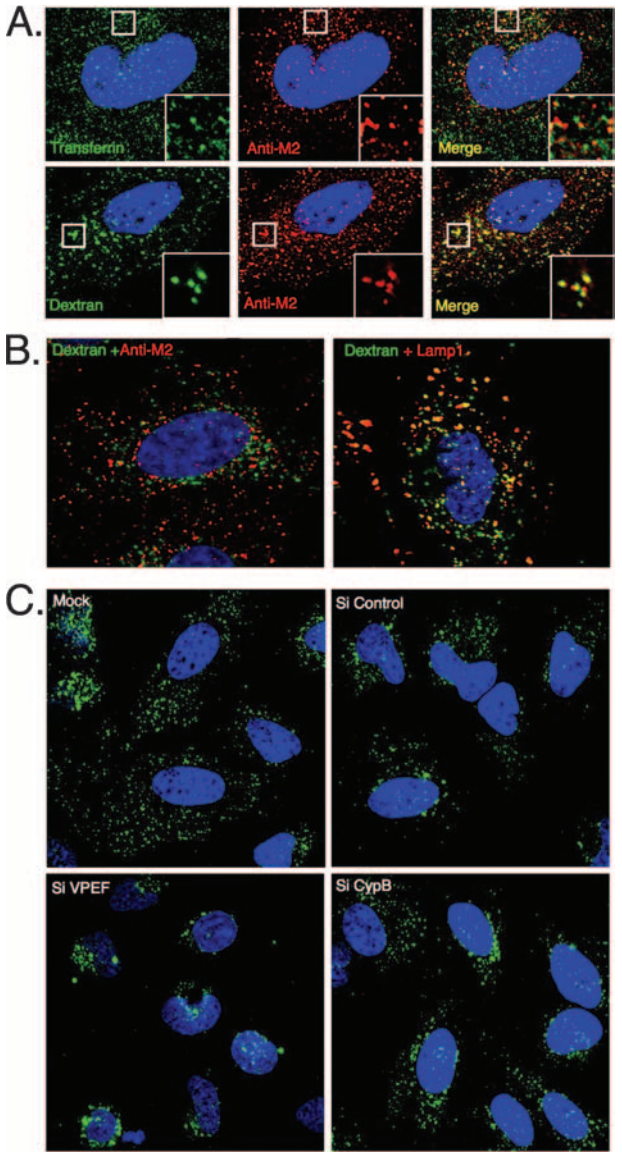

FIG. 6. VPEF mediates fluid phase endocytosis. (A) Intracellular VPEF colocalized with internalized dextran but not with transferrin. HeLa cells were incubated with fluorescence-labeled transferrin or dextran at 37°C as described in Materials and Methods, fixed, permeabilized, and stained for endogenous VPEF. The insets in the panels show enlarged views of the areas outlined by the white squares. (B) No colocalization of VPEF with dextran when the latter was transported to lysosomes. HeLa cells were pulsed for 40 min with fluorescence-conjugated dextran and chased for 4 h at 37°C. The fluorescence-conjugated dextran became segregated from VPEF (left) and moved to the late endosome compartments, which were stained by anti-Lamp1 (lysosomal marker) Abs (right). (C) Knockdown of VPEF expression interrupted dextran uptake in HeLa cells. HeLa cells were mock-transfected (mock) or transfected with control siRNA (Si control), CypB siRNA (Si CypB), or VPEF 3-378 siRNA (Si VPEF) as described above, incubated with fluorescence-labeled dextran for 1 h at 37°C, washed, and then fixed for confocal microscopy analyses.

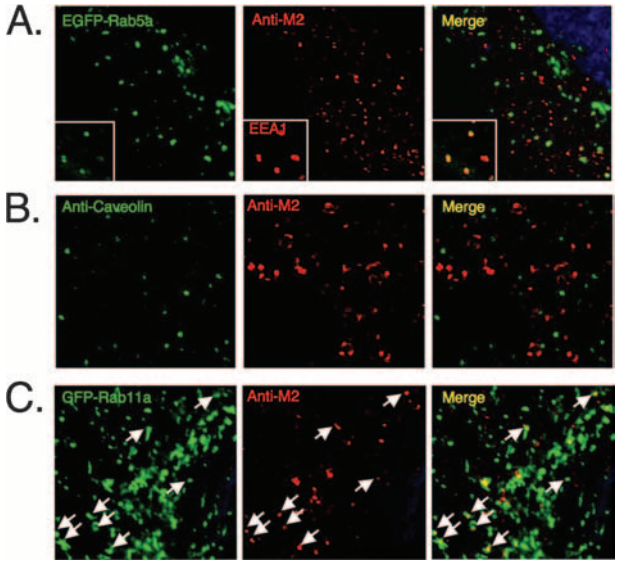

FIG. 7. No colocalization of intracellular VPEF with the Rab5a-containing early endosome compartments (A) or caveolin-1-containing caveosomes (B) in HeLa cells. The small insets in panel A show good colocalization of Rab5a with EEA1, an early endosome marker. (C) Intracellular VPEF partially colocalized with the Rab11-containing recycling endosome compartment in HeLa cells. EGFP, enhanced GFP.

hands, DN-Dyn2 blocked transferrin uptake but not IMV entry; we suspect that a higher level of DN-Dyn2 is needed to block virus entry than to block ligand uptake. Alternatively, endogenous dynamin in HeLa cells may contain splicing variants that interacted with DN-Dyn1 and DN-Dyn2 with different affinities. It is worth noting that, despite a clear function of dynamin in clathrin- and caveola-mediated coated-vesicle formation, its role in coat-independent endocytosis processes such as fluid uptake has been controversial (1, 17, 18, 23, 24, 35). Four splicing variants of dynamin 2 have been reported (8, 54), and the DN GTPase mutants of all four splicing variants blocked transferrin uptake well; however, only two splicing variants blocked dextran uptake, suggesting differential functions of the distinct splicing variants in fluid uptake (7). Furthermore, we identified and characterized VPEF, a novel cellular protein that is important for vaccinia IMV penetration into HeLa cells. Our data also suggested that VPEF and dynamin mediate IMV penetration through different mechanisms. How VPEF interacts with viral components to allow penetration remains to be clarified in the future. VPEF mRNA was detected in many mammalian cell lines (data not shown), suggesting a conserved function for VPEF. This would not be too surprising, given the wide host infectivity of vaccinia virus; while we demonstrated the importance of VPEF in HeLa cells, it remains to be determined whether the same conclusion will apply to other cell types. It also awaits more experiments to determine whether the extracellular form of vaccinia virus requires VPEF for cell entry or not.

Because vaccinia virus attachment to cells at 4°C was relatively inefficient and only 1 to 2% of the input viral particles bound to cells after a 60-min incubation (37), we had to use relatively high-MOI (MOI = 40 to 100) infections in the EM and confocal analyses. Using viral early gene expression assays, we observed that vaccinia IMV entry into HeLa cells remained sensitive to BFLA in low-MOI (MOI = 0.1 to 5) infections, supporting the idea that MOI per se did not dictate the cell entry pathways employed by viruses. It is also worth noting that

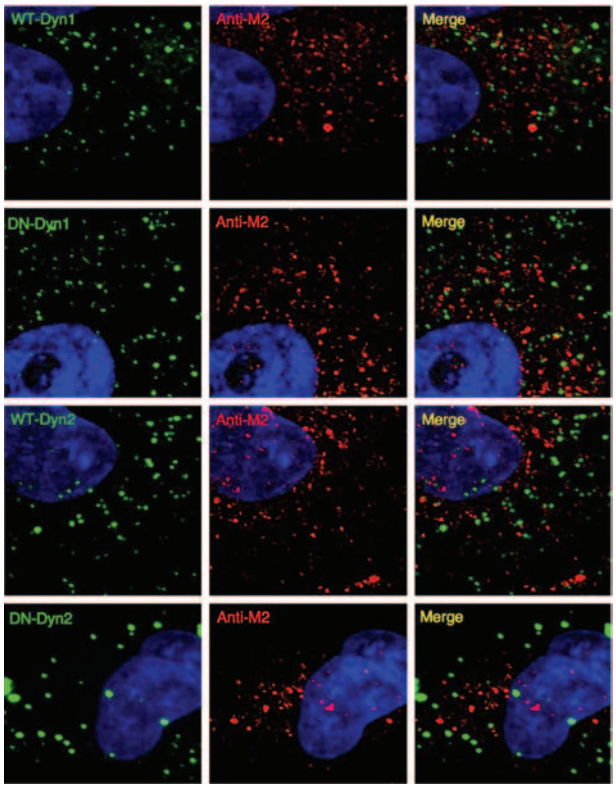

FIG. 8. No colocalization of dynamin with VPEF in HeLa cells. HeLa cells were transfected with GFP-fused WT-Dyn1, WT-Dyn2, DN-Dyn-1, or DN-Dyn2, permeabilized, and stained with anti-M2 Abs.

endocytosis of the WR strain of vaccinia IMV into HeLa cells, as described here, is not simply an artifact of high-MOI infections since infections of cells with the IHD-J strain of vaccinia IMV at a high MOI of 200 to 300 did not result in obvious endocytosis into BSC-1 (58) and HeLa cells (37).

In summary, these results demonstrate that vaccinia IMV is able to pirate cellular actin to get closer to cell bodies and manages to enter cells by hijacking a ubiquitous VPEF-dependent fluid transport pathway that is part of these cells' normal repertoire. We hypothesize that VPEF represents a new cargo or component of the earliest acceptor compartment of the clathrin- and caveolin-independent vesicle trafficking system (41) for the uptake of bulk phase fluid. The verification of this hypothesis will require further study.

ACKNOWLEDGMENTS

We thank Alice Dautry-Varsat, Sandra Schmid, Roger Y. Tsien, and Marino Zerial for providing the plasmids. We also thank Tomas Kirchhausen for providing dynasore.

This work was supported by grants from the Academia Sinica and the National Science Council (NSC96-2627-M-001-004), Taiwan.

REFERENCES

1. **Altschuler, Y., S. M. Barbas, L. J. Terlecky, K. Tang, S. Hardy, K. E. Mostov, and S. L. Schmid.** 1998. Redundant and distinct functions for dynamin-1 and dynamin-2 isoforms. J. Cell Biol. **143:**1871–1881.
2. **Andrade, A. A., P. N. Silva, A. C. Pereira, L. P. De Sousa, P. C. Ferreira, R. T. Gazzinelli, E. G. Kroon, C. Ropert, and C. A. Bonjardim.** 2004. The vaccinia virus-stimulated mitogen-activated protein kinase (MAPK) pathway is required for virus multiplication. Biochem. J. **381:**437–446.
3. **Armstrong, J. A., D. H. Metz, and M. R. Young.** 1973. The mode of entry of vaccinia virus into L cells. J. Gen. Virol. **21:**533–537.
4. **Bair, C. H., C. S. Chung, I. A. Vasilevskaya, and W. Chang.** 1996. Isolation and characterization of a Chinese hamster ovary mutant cell line with altered sensitivity to vaccinia virus killing. J. Virol. **70:**4655–4666.
5. **Bayer, N., D. Schober, E. Prchla, R. F. Murphy, D. Blaas, and R. Fuchs.** 1998. Effect of bafilomycin A1 and nocodazole on endocytic transport in HeLa cells: implications for viral uncoating and infection. J. Virol. **72:**9645–9655.
6. **Benmerah, A., M. Bayrou, N. Cerf-Bensussan, and A. Dautry-Varsat.** 1999. Inhibition of clathrin-coated pit assembly by an Eps15 mutant. J. Cell Sci. **112**(Pt. 9)**:**1303–1311.
7. **Cao, H., J. Chen, M. Awoniyi, J. R. Henley, and M. A. McNiven.** 2007. Dynamin 2 mediates fluid-phase micropinocytosis in epithelial cells. J. Cell Sci. **120:**4167–4177.
8. **Cao, H., F. Garcia, and M. A. McNiven.** 1998. Differential distribution of dynamin isoforms in mammalian cells. Mol. Biol. Cell **9:**2595–2609.
9. **Chang, A., and D. H. Metz.** 1976. Further investigations on the mode of entry of vaccinia virus into cells. J. Gen. Virol. **32:**275–282.
10. **Chiu, W. L., C. L. Lin, M. H. Yang, D. L. Tzou, and W. Chang.** 2007. Vaccinia virus 4c (A26L) protein on intracellular mature virus binds to the extracellular cellular matrix laminin. J. Virol. **81:**2149–2157.
11. **Chung, C. S., C. H. Chen, M. Y. Ho, C. Y. Huang, C. L. Liao, and W. Chang.** 2006. Vaccinia virus proteome: identification of proteins in vaccinia virus intracellular mature virion particles. J. Virol. **80:**2127–2140.
12. **Chung, C. S., J. C. Hsiao, Y. S. Chang, and W. Chang.** 1998. A27L protein mediates vaccinia virus interaction with cell surface heparan sulfate. J. Virol. **72:**1577–1585.
13. **Chung, C. S., C. Y. Huang, and W. Chang.** 2005. Vaccinia virus penetration requires cholesterol and results in specific viral envelope proteins associated with lipid rafts. J. Virol. **79:**1623–1634.
14. **Condit, R. C., N. Moussatche, and P. Traktman.** 2006. In a nutshell: structure and assembly of the vaccinia virion. Adv. Virus Res. **66:**31–124.
15. **Cook, T. A., R. Urrutia, and M. A. McNiven.** 1994. Identification of dynamin 2, an isoform ubiquitously expressed in rat tissues. Proc. Natl. Acad. Sci. USA **91:**644–648.
16. **Dales, S., and R. Kajioka.** 1964. The cycle of multiplication of vaccinia virus in Earle's strain L cells. I. Uptake and penetration. Virology **24:**278–294.
17. **Damke, H., T. Baba, A. M. van der Bliek, and S. L. Schmid.** 1995. Clathrin-independent pinocytosis is induced in cells overexpressing a temperature-sensitive mutant of dynamin. J. Cell Biol. **131:**69–80.
18. **Damke, H., T. Baba, D. E. Warnock, and S. L. Schmid.** 1994. Induction of mutant dynamin specifically blocks endocytic coated vesicle formation. J. Cell Biol. **127:**915–934.
19. **Doms, R. W., R. Blumenthal, and B. Moss.** 1990. Fusion of intra- and extracellular forms of vaccinia virus with the cell membrane. J. Virol. **64:**4884–4892.
20. **Fenner, F.** 1990. Poxviruses, p. 2113–2133. *In* B. Fields and D. M. Knipe (ed.), Virology. Raven Press, New York, NY.
21. **Gold, E. S., D. M. Underhill, N. S. Morrissette, J. Guo, M. A. McNiven, and A. Aderem.** 1999. Dynamin 2 is required for phagocytosis in macrophages. J. Exp. Med. **190:**1849–1856.
22. **Guarner, J., B. J. Johnson, C. D. Paddock, W. J. Shieh, C. S. Goldsmith, M. G. Reynolds, I. K. Damon, R. L. Regnery, and S. R. Zaki.** 2004. Monkeypox transmission and pathogenesis in prairie dogs. Emerg. Infect. Dis. **10:**426–431.
23. **Guha, A., V. Sriram, K. S. Krishnan, and S. Mayor.** 2003. Shibire mutations reveal distinct dynamin-independent and -dependent endocytic pathways in primary cultures of *Drosophila* hemocytes. J. Cell Sci. **116:**3373–3386.
24. **Herskovits, J. S., C. C. Burgess, R. A. Obar, and R. B. Vallee.** 1993. Effects of mutant rat dynamin on endocytosis. J. Cell Biol. **122:**565–578.
25. **Ho, S. N., H. D. Hunt, R. M. Horton, J. K. Pullen, and L. R. Pease.** 1989. Site-directed mutagenesis by overlap extension using the polymerase chain reaction. Gene **77:**51–59.
26. **Hsiao, J.-C., C.-S. Chung, and W. Chang.** 1998. Cell surface proteoglycans are necessary for A27L protein-mediated cell fusion: identification of the N-terminal region of A27L protein as the glycosaminoglycan-binding domain. J. Virol. **72:**8374–8379.
27. **Hsiao, J. C., C. S. Chung, and W. Chang.** 1999. Vaccinia virus envelope D8L protein binds to cell surface chondroitin sulfate and mediates the adsorption of intracellular mature virions to cells. J. Virol. **73:**8750–8761.
28. **Hung, J. J., M. T. Hsieh, M. J. Young, C. L. Kao, C. C. King, and W. Chang.** 2004. An external loop region of domain III of dengue virus type 2 envelope protein is involved in serotype-specific binding to mosquito but not mammalian cells. J. Virol. **78:**378–388.
29. **Hybiske, K., and R. S. Stephens.** 2007. Mechanisms of *Chlamydia trachomatis* entry into nonphagocytic cells. Infect. Immun. **75:**3925–3934.
30. **Ichihashi, Y., and M. Oie.** 1996. Neutralizing epitope on penetration protein of vaccinia virus. Virology **220:**491–494.
31. **Izmailyan, R. A., C. Y. Huang, S. Mohammad, S. N. Isaacs, and W. Chang.** 2006. The envelope G3L protein is essential for entry of vaccinia virus into host cells. J. Virol. **80:**8402–8410.
32. **Joklik, W. K.** 1962. The purification of four strains of poxvirus. Virology **18:**9–18.

33. **Kaiser, J.** 2007. Smallpox vaccine. A tame virus runs amok. Science **316:** 1418–1419.
34. **Kent, S., R. De Rose, and E. Rollman.** 2007. Drug evaluation: DNA/MVA prime-boost HIV vaccine. Curr. Opin. Investig. Drugs **8:**159–167.
35. **Kosaka, T., and K. Ikeda.** 1983. Reversible blockage of membrane retrieval and endocytosis in the garland cell of the temperature-sensitive mutant of *Drosophila melanogaster*, shibirets1. J. Cell Biol. **97:**499–507.
36. **Lehmann, M. J., N. M. Sherer, C. B. Marks, M. Pypaert, and W. Mothes.** 2005. Actin- and myosin-driven movement of viruses along filopodia precedes their entry into cells. J. Cell Biol. **170:**317–325.
37. **Locker, J. K., A. Kuehn, S. Schleich, G. Rutter, H. Hohenberg, R. Wepf, and G. Griffiths.** 2000. Entry of the two infectious forms of vaccinia virus at the plasma membane is signaling-dependent for the IMV but not the EEV. Mol. Biol. Cell **11:**2497–2511.
38. **Macia, E., M. Ehrlich, R. Massol, E. Boucrot, C. Brunner, and T. Kirchhausen.** 2006. Dynasore, a cell-permeable inhibitor of dynamin. Dev. Cell **10:**839–850.
39. **Mallardo, M., S. Schleich, and J. Krijnse Locker.** 2001. Microtubule-dependent organization of vaccinia virus core-derived early mRNAs into distinct cytoplasmic structures. Mol. Biol. Cell **12:**3875–3891.
40. **Marks, B., M. H. Stowell, Y. Vallis, I. G. Mills, A. Gibson, C. R. Hopkins, and H. T. McMahon.** 2001. GTPase activity of dynamin and resulting conformation change are essential for endocytosis. Nature **410:**231–235.
41. **Mayor, S., and R. E. Pagano.** 2007. Pathways of clathrin-independent endocytosis. Nat. Rev. Mol. Cell Biol. **8:**603–612.
42. **Oh, P., D. P. McIntosh, and J. E. Schnitzer.** 1998. Dynamin at the neck of caveolae mediates their budding to form transport vesicles by GTP-driven fission from the plasma membrane of endothelium. J. Cell Biol. **141:**101–114.
43. **Pelkmans, L., J. Kartenbeck, and A. Helenius.** 2001. Caveolar endocytosis of simian virus 40 reveals a new two-step vesicular-transport pathway to the ER. Nat. Cell Biol. **3:**473–483.
44. **Rahbar, R., T. T. Murooka, A. A. Hinek, C. L. Galligan, A. Sassano, C. Yu, K. Srivastava, L. C. Platanias, and E. N. Fish.** 2006. Vaccinia virus activation of CCR5 invokes tyrosine phosphorylation signaling events that support virus replication. J. Virol. **80:**7245–7259.
45. **Resch, W., K. K. Hixson, R. J. Moore, M. S. Lipton, and B. Moss.** 2007. Protein composition of the vaccinia virus mature virion. Virology **358:**233–247.
46. **Reynolds, E.** 1963. The use of lead citrate at high pH as an electron-opaque stain in electron microscopy. J. Cell Biol. **55:**541–552.
47. **Roy, S., R. Luetterforst, A. Harding, A. Apolloni, M. Etheridge, E. Stang, B. Rolls, J. F. Hancock, and R. G. Parton.** 1999. Dominant-negative caveolin inhibits H-Ras function by disrupting cholesterol-rich plasma membrane domains. Nat. Cell Biol. **1:**98–105.

47a. **Sambrook, J., and D. W. Russell.** 2001. Molecular cloning: a laboratory manual, 3rd ed. Cold Spring Harbor Laboratory Press, Cold Spring Harbor, NY.

48. **Schwartz, S. L., C. Cao, O. Pylypenko, A. Rak, and A. Wandinger-Ness.** 2007. Rab GTPases at a glance. J. Cell Sci. **120:**3905–3910.
49. **Senkevich, T. G., B. M. Ward, and B. Moss.** 2004. Vaccinia virus A28L gene encodes an essential protein component of the virion membrane with intramolecular disulfide bonds formed by the viral cytoplasmic redox pathway. J. Virol. **78:**2348–2356.
50. **Senkevich, T. G., B. M. Ward, and B. Moss.** 2004. Vaccinia virus entry into cells is dependent on a virion surface protein encoded by the A28L gene. J. Virol. **78:**2357–2366.
51. **Shaner, N. C., R. E. Campbell, P. A. Steinbach, B. N. Giepmans, A. E. Palmer, and R. Y. Tsien.** 2004. Improved monomeric red, orange and yellow fluorescent proteins derived from *Discosoma* sp. red fluorescent protein. Nat. Biotechnol. **22:**1567–1572.
52. **Short, J. M., J. M. Fernandez, J. A. Sorge, and W. D. Huse.** 1988. Lambda ZAP: a bacteriophage lambda expression vector with in vivo excision properties. Nucleic Acids Res. **16:**7583–7600.
53. **Singh, R. D., V. Puri, J. T. Valiyaveettil, D. L. Marks, R. Bittman, and R. E. Pagano.** 2003. Selective caveolin-1-dependent endocytosis of glycosphingolipids. Mol. Biol. Cell **14:**3254–3265.
54. **Sontag, J. M., E. M. Fykse, Y. Ushkaryov, J. P. Liu, P. J. Robinson, and T. C. Sudhof.** 1994. Differential expression and regulation of multiple dynamins. J. Biol. Chem. **269:**4547–4554.
55. **Spiegel, S., S. Kassis, M. Wilchek, and P. H. Fishman.** 1984. Direct visualization of redistribution and capping of fluorescent gangliosides on lymphocytes. J. Cell Biol. **99:**1575–1581.
56. **Spurr, A.** 1969. A low-viscosity epoxy resin embedding medium for electron microscopy. J. Ultrastruct. Res. **26:**31–43.
57. **Stanford, M. M., and G. McFadden.** 2007. Myxoma virus and oncolytic virotherapy: a new biologic weapon in the war against cancer. Expert Opin. Biol. Ther. **7:**1415–1425.
58. **Townsley, A. C., A. S. Weisberg, T. R. Wagenaar, and B. Moss.** 2006. Vaccinia virus entry into cells via a low-pH-dependent endosomal pathway. J. Virol. **80:**8899–8908.
59. **Ullrich, O., S. Reinsch, S. Urbe, M. Zerial, and R. G. Parton.** 1996. Rab11 regulates recycling through the pericentriolar recycling endosome. J. Cell Biol. **135:**913–924.
60. **van der Bliek, A. M., T. E. Redelmeier, H. Damke, E. J. Tisdale, E. M. Meyerowitz, and S. L. Schmid.** 1993. Mutations in human dynamin block an intermediate stage in coated vesicle formation. J. Cell Biol. **122:**553–563.
61. **Vanderplasschen, A., M. Hollinshead, and G. L. Smith.** 1997. Antibodies against vaccinia virus do not neutralize extracellular enveloped virus but prevent virus release from infected cells and comet formation. J. Gen. Virol. **78:**2041–2048.
62. **Vanderplasschen, A., M. Hollinshead, and G. L. Smith.** 1998. Intracellular and extracellular vaccinia virions enter cells by different mechanisms. J. Gen. Virol. **79**(Pt. 4)**:**877–887.
63. **Vanderplasschen, A., and G. L. Smith.** 1997. A novel virus binding assay using confocal microscopy: demonstration that the intracellular and extracellular vaccinia virions bind to different cellular receptors. J. Virol. **71:**4032–4041.
64. **Walter, R. J., R. D. Berlin, J. R. Pfeiffer, and J. M. Oliver.** 1980. Polarization of endocytosis and receptor topography on cultured macrophages. J. Cell Biol. **86:**199–211.
65. **Yoder, J. D., T. S. Chen, C. R. Gagnier, S. Vemulapalli, C. S. Maier, and D. E. Hruby.** 2006. Pox proteomics: mass spectrometry analysis and identification of vaccinia virion proteins. Virol. J. **3:**10.